Roman KRÓL 📧 [1]

Analysis of the single stage cycloidal gearbox with lobe defects.
Fault diagnosis attempts using coherence function and Morris minimum-bandwidth wavelets

In this article, the frequency characteristics of the forces and torques in the various cycloidal gearbox designs were investigated. The aim of the article is the search for frequency patterns that could be used in the formulation of a fault diagnosis methodology. Numerical analysis was performed in the cycloidal gearbox without defects as well as in cycloidal gearboxes with lobe defects or with removed lobes. The results of the numerical analysis were obtained in the multibody dynamics model of the cycloidal gearbox, implemented in Fortran and using the 2nd-order Runge-Kutta method for the integration of the motion equations. The used model is planar and uses Hunt and Crossley's nonlinear contact modelling algorithm, which was modified using the Heaviside function and backlash to fit cycloidal gearbox model convergence demands. In the analysis of fault diagnosis methods, the coherence function and Morris minimum-bandwidth wavelets were used. It is difficult to find a unique pattern in the results to use in the fault diagnosis because of the random characteristics of the torques at the input and output shafts. Based on obtained results, a promising, low-vibration cycloidal gearbox design with removed 7 lobes of the single wheel was studied using the FFT algorithm.

1. Introduction

Fault diagnosis is a developing research branch, rising to new levels with improvements in neural networks and wavelets. Using statistics, digital signal processing, wavelets, neural networks or spectral analysis researchers look for methods

📧 Roman KRÓL, e-mail: r.krol@uthrad.pl

[1]Faculty of Mechanical Engineering, Kazimierz Pulaski University of Technology and Humanities in Radom, Poland; ORCID: 0000-0002-6279-9562

of presentation and selection of the specified signal features identifying defects. The signals are measured and processed by microcontrollers and processors of newer generations allowing for faster analysis and application of the new algorithms [1, 2].

Methods of gearbox diagnostics are often based on the entities concerning the rotational motion of shafts. It may be angle of rotation, angular speed, angular acceleration and input or output torque. In cycloidal gearboxes, the output torque is a random signal. In the models of cycloidal gearbox programmed using mathematical software or various computer programming languages, the important role plays contact modelling. In advanced models, nonlinear dependence between penetration, force and energy dissipation appears, which influences other dynamical parameters of gearbox parts (angular velocity and angular acceleration of the cycloidal wheels, input and output shafts). These nonlinear dependences lead to an unpredictable random form of the output torque and difficulties in the extraction of the defect-identifying signal features.

Successful fault diagnosis of the cycloidal gearbox was presented in [3], where multifractal analysis of the vertical vibrations by the wavelet leader method was performed. Analysis of the log-cumulants in [3] allowed for a distinction between a healthy gearbox and one containing fault in general.

In works [4, 5], which concern topic of the dynamic analysis and backlash it was mentioned, that developing a multibody dynamics model of the cycloidal gearbox with contact modelling is difficult and complex. Research on the improvement of the cycloidal gearbox models lead to the implementation in the Fortran programming language the parametrized cycloidal gearbox model for transient analysis [6–8]. This model allows for modification of the geometry of the gearbox as well as the contact and dynamic parameters. The feature of geometry modification allows for the application of the mentioned models in fault diagnosis. Studying the spectral characteristics and time courses of the dynamical entities in the cycloidal gearbox [4–6, 9] built the motivation for searching features in the spectrum of the output torque and origins of the specified elements of the spectrum. Revealing the meaning of the given beans in the spectrum allows for the application of this knowledge in the fault diagnosis.

Contemporary works concerning this topic are [10, 11], where kinematical error and contact were studied. In [12], the distributed wear in the planetary gearbox was analysed in the scope of fault diagnosis, in [13–15] analysis of the gearboxes with removed teeth was performed and [16–21] concern other defects in the gearboxes.

Works that deal with application of the advanced methods in studying spectral characteristics of cycloidal gearboxes are rare [3].

In this article, the search for the frequency features, which characterize the defect in the specified lobe has been carried out. Based on the methodology presented in [18, 22], the MATLAB coherence function was used to find the influence of the defect in the single lobe on the output torque frequency spectrum. It will be shown in the results chapter of this article, that the coherence function is not

precise enough to identify the defect located in the specified lobe. The next step in the analysis, arising from too little information in the coherence functions, is to check the distribution of the multiple frequency levels of the output torque in the time domain. This step can be done by the application of wavelets. MATLAB include a high number of predefined wavelets, 130 of which were applied to compute scalograms of the output torque and it was still difficult to find explicit dependence between localization of defect and scalogram features. Significant changes have been found only in the Morris minimum-bandwidth wavelet "mb32.3" [23]. The research presented in this article not only concerns fault diagnosis topics.

Based on obtained results, the numerical models of new designs of the cycloidal gearbox were tested. Many scalograms for various wavelets showed a reduction of the high-frequency components in the gearbox with 7 and 4 consecutive lobes removed. In the gearbox with 8 removed lobes and with 2nd, 4th, 6th and 8th lobes removed high temporary vibrations occurred due to locking of the gearbox. These high amplitudes affect the calculation of scalograms and do not show dependencies similar to other scalograms. Based on the fact, that high frequencies are reduced in the gearbox set-ups with 7 removed lobes, two new designs were constructed: the first with 7 consecutive lobes removed in a single cycloidal wheel, and the second with 7 consecutive lobes removed in both wheels. The gearbox in the second model was locked and the analysis of this model was not convergent. The first model showed a promising reduction of the high-vibration components in the output torque spectrum. The drawback of this design is increased forces at the internal sleeves.

2. Analysed gearbox

The analysed single-stage cycloidal gearbox consists of input and output shafts, two cycloidal wheels, 16 external sleeves and 8 internal sleeves. The shape of both cycloidal wheels is the same and it is described in parametric equations (1) with entities given in Table 1. The wheels are counter-rotated by 180°. The results visualization software was implemented in Java, using LWJGL (Light Weight Java Game Library) with OpenGL. The visualization software does not show input and output shafts with eccentric cams, on which cycloidal wheels are mounted. The external sleeves are mounted in the ring, they are fixed and can rotate around their longitudinal axis. The internal sleeves are mounted in the output shaft. The following modifications of the presented design were studied: the models 1–8 with wear defects of the consecutive 1–8 lobes. Each wear defect was introduced to the cycloidal wheel by zeroing the parametric coordinates of the cycloidal wheel in the range of 0–12° for each lobe. The gap was next substituted by the linear function connecting boundary points of the zeroed region. This kind of defect is a simulation of the wear of half of the lobe due to friction. The additional models with a) 1st and 5th, b) 1st, 4th and 7th c) 1st, 3rd, 5th and 7th, d) 2nd, 4th, 6th and 8th worn lobes were also studied. After all presented analyses, two models with completely removed 7

consecutive lobes in a) single wheel and b) both wheels were analysed to check the elimination of the high frequencies in the cycloidal gearbox. The model with 8 consecutive worn lobes is presented in Fig. 1.

$$u(\alpha) = \frac{ez_k}{m}\cos(\alpha) + e\cos(z_k\alpha) - q\cos(\alpha + \gamma),$$

$$v(\alpha) = \frac{ez_k}{m}\sin(\alpha) + e\sin(z_k\alpha) - q\sin(\alpha + \gamma),$$

$$\gamma = \mathrm{atan}\left[\frac{\sin(z_s\alpha)}{\frac{1}{m} + \cos(z_s\alpha)}\right].$$

(1)

Table 1. Parameters used in the equation (1)

Parameter	Description	Value
$u(\alpha)$	Horizontal coordinate	–
$v(\alpha)$	Vertical coordinate	–
α [rad]	Equation parameter	0–2π
e [m]	Eccentricity	0.0028
z_k	Number of external sleeves	16
z_s	Number of lobes	15
m	Short-width coefficient	0.7
q [m]	Radius of the external sleeve	0.006
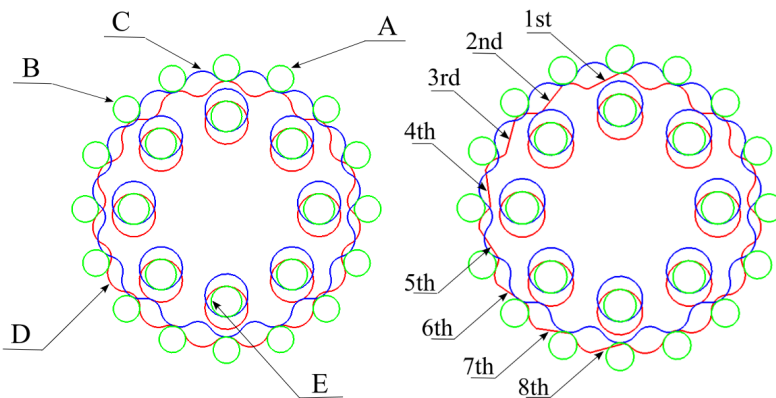
Fig. 1. Analysed model of the cycloidal gearbox. The model without defects (left) and the model with 8 consecutive worn lobes (1st-8th) (right). A – designates the 1st external sleeve, B – designates the 14th external sleeve, C – designates the external cycloidal wheel, D – designates the internal cycloidal wheel and E – designates the internal sleeve

www.czasopisma.pan.pl PAN www.journals.pan.pl
POLSKA AKADEMIA NAUK

Analysis of the single stage cycloidal gearbox with lobe defects. Fault diagnosis. . .   413

The masses and moments of inertia of the cycloidal gearbox parts used in the analysis are shown in Table 2. Table 3 contains values of drives and loads. The dimensions of the cycloidal gearbox are shown in Fig. 2.

Table 2. Mechanical parameters of the cycloidal gearbox parts. The moments of inertia have been calculated relative to the given part's centre of mass

Body	Model parameters	
	Mass [kg]	Moment of inertia [kg m^2]
Input shaft	0.2341	$1.846 \cdot 10^{-6}$
Output shaft	1.6345	$1.373 \cdot 10^{-4}$
Cycloidal wheel	0.5998	$1.57538 \cdot 10^{-4}$
Internal sleeve	0.048	$1.1013 \cdot 10^{-5}$
External sleeve	0.048	$1.1013 \cdot 10^{-5}$

Table 3. Drives and loads of the cycloidal gearbox

Entity	Value
Angular velocity of the input shaft [Hz; rad/s; RPM]	8.33; 52.34; 500
Torque applied at the output shaft [Nm]	22
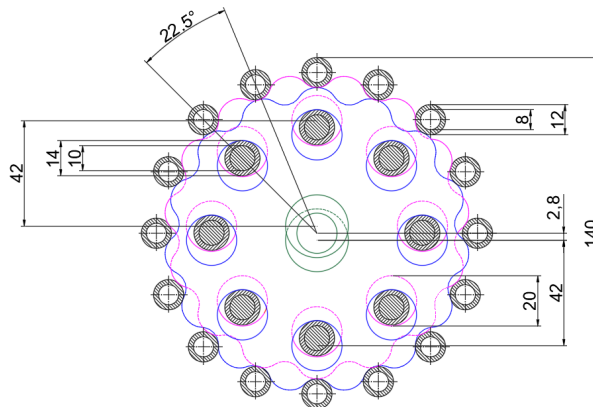
Fig. 2. Dimensions of the cycloidal gearbox used in the analysis [6]

3. Multibody dynamics model of the cycloidal gearbox implemented in Fortran programming language

Multibody dynamics analysis of the cycloidal gearbox has been performed using software [24] described in [6]. The modification of the mentioned software was done including the start of the cycloidal gearbox from the rest position. The contact

modelling algorithm was also modified aiming to correct energy dissipation. In
the multibody analysis, equation (2) is solved in each iteration of the Runge-Kutta
algorithm.

$$\begin{bmatrix} \mathbf{M} & -\mathbf{D}^T \\ \mathbf{D} & \mathbf{0} \end{bmatrix} \begin{bmatrix} \ddot{\mathbf{u}} \\ \lambda \end{bmatrix} = \begin{bmatrix} \mathbf{F} \\ \gamma \end{bmatrix}, \tag{2}$$

where: $\mathbf{M}$ – mass matrix (contains masses and moments of inertia of the parts),
$\mathbf{D}$ – Jacobian matrix, $\mathbf{0}$ – zero matrix, $\ddot{\mathbf{u}}$ – solved accelerations, λ – solved reaction
forces, $\mathbf{F}$ – vector of applied forces and moments, γ – right-hand side vector of the
acceleration equations.

The mass matrix contains masses and moments of inertia specified in Table 2.
Jacobian matrix was formulated similarly to the model presented in [6] including
the driver-joint. The exceptions in the multibody model concern the right-hand
side acceleration vector γ, applied forces vector $\mathbf{F}$, geometric constraints vector
and velocity constraints vector. Entities γ and $\mathbf{F}$ are parts of the right-hand side
in the system of equations (2). The geometry constraints and velocity constraints
vectors are used in the initial conditions correction subroutine. The drive of the
input shaft has been defined using the following modifications (3)–(5) relative to
the model [6, 24]. The cycloidal gearbox consists of 28 bodies (2 shafts, 2 cycloidal
wheels, 8 internal sleeves and 16 external sleeves). There are 2 constraint equations
for each body in the multibody dynamics model $(28 \cdot 2)$ and the last constraint is the
rotational driver joint (57th constraint equation). The first body is the input shaft.
It has three coordinates in the planar dynamics: two linear displacements x and y
and the angular displacement φ. The third component of the displacement vector
u is the angular displacement of the input shaft.

$$\Phi_{28 \cdot 2 + 1} = u_3 - f(t), \tag{3}$$

$$V_{28 \cdot 2 + 1} = f'(t), \tag{4}$$

$$\gamma_{28 \cdot 2 + 1} = f''(t), \tag{5}$$

where: Φ – constraints vector, u – displacements vector, V – velocity constraints
vector, γ – right-hand side accelerations vector, $f(t)$, $f'(t)$, $f''(t)$ – designates the
driver function and its derivatives (6)–(8).

$$f(t) = \begin{cases} t < 0.2 \text{ s} & \Rightarrow \ 0.5 \cdot 261.8 \cdot t^2, \\ t \geqslant 0.2 \text{ s} & \Rightarrow \ 52.36 \cdot t, \end{cases} \tag{6}$$

$$f'(t) = \begin{cases} t < 0.2 \text{ s} & \Rightarrow \ 261.8 \cdot t, \\ t \geqslant 0.2 \text{ s} & \Rightarrow \ 52.36, \end{cases} \tag{7}$$

$$f''(t) = \begin{cases} t < 0.2 \text{ s} & \Rightarrow 261.8, \\ t \geqslant 0.2 \text{ s} & \Rightarrow \ 0, \end{cases} \tag{8}$$

where: t – time [s], value 52.36 is given in [rad/s] and value 261.8 in [rad/s^2].

www.czasopisma.pan.pl   PAN   www.journals.pan.pl

POLSKA AKADEMIA NAUK

Analysis of the single stage cycloidal gearbox with lobe defects. Fault diagnosis. . .   415

The load of the output shaft was also modified to rise from the rest state to the constant value $T_{\text{out}} = 22$ Nm. The second body is the output shaft. The 6th coordinate of the applied force vector is the torque (9) applied at the output shaft.

$$F_6 = l(t), \tag{9}$$

where $l(t)$ is time function defined in (10).

$$l(t) = \begin{cases} t < 0.2 \text{ s} & \Rightarrow & 110 \cdot t, \\ t \geqslant 0.2 \text{ s} & \Rightarrow & 22, \end{cases} \tag{10}$$

where: value 110 is given in [Nm/s], value 22 is in [Nm] and t is in [s].

The contact modelling algorithm has been modified to distinguish if the contact points' relative velocity has a positive or negative value. This approach allows for guaranteeing energy dissipation during unloading (11).

$$F_N = \begin{cases} v_{nzj} < 0 & \Rightarrow & K_{pc} \cdot \delta^{1.5} - C_{pc} \cdot \left| v_{nzj} \right|, \\ v_{nzj} > 0 & \Rightarrow & K_{pc} \cdot \delta^{1.5} + C_{pc} \cdot \left| v_{nzj} \right|, \end{cases} \tag{11}$$

where: F_N – contact normal force, v_{nzj} – relative velocity of the contact points, K_{pc} – contact stiffness (this parameter depend on the surface curvature of the contacting bodies), δ – penetration depth, C_{pc} – contact damping.

The contact stiffness and contact damping are modelled using Heaviside step function (12)–(13).

$$K_{pc} = \begin{cases} \delta < 0 & \Rightarrow & 0, \\ \delta \in (0; 0.00001) & \Rightarrow & \dfrac{K_{pc\,\text{max}}}{0.00001} \delta, \\ \delta > 0.00001 & \Rightarrow & K_{pc\,\text{max}}, \end{cases} \tag{12}$$

$$C_{pc} = \begin{cases} \delta < 0 & \Rightarrow & 0, \\ \delta \in (0; 0.00001) & \Rightarrow & \dfrac{C_{pc\,\text{max}}}{0.00001} \delta, \\ \delta > 0.00001 & \Rightarrow & C_{pc\,\text{max}}, \end{cases} \tag{13}$$

where: $K_{pc\,\text{max}}$ is the value of the contact stiffness calculated from (14) [11, 25] and $C_{pc\,\text{max}}$ is 150 [Ns/m] [8].

$$K_{pc\,\text{max}} = \frac{4H}{3\pi(h_c + h_p)} \sqrt{\frac{R_c R_p}{R_c + R_p}}, \tag{14}$$

where: R_c, R_p – designates curvature radiuses of the cycloidal wheel and external sleeve respectively, $H = 0.01$ is the scale coefficient of the contact stiffness, h_c and

h_p are given in (15) and 16).

$$h_c = \frac{1 - v_c^2}{\pi E_c}, \tag{15}$$

$$h_p = \frac{1 - v_p^2}{\pi E_p}, \tag{16}$$

where: v_c, v_p – Poisson ratios of the cycloidal wheel and external sleeves material respectively, E_c, E_p – Young moduli of the cycloidal wheel and external sleeves material respectively.

4. Designs of the cycloidal gearbox with artificial wear defects

It was mentioned in section 2, that wear of the single lobe has been modelled by the removal of half of the lobe and substitution of the removed part by the linear function connecting both ends in the remained part of the cycloid. Eight analyses have been performed for the artificial wear defect introduction to the consecutive lobes. The results of the analyses (the forces acting on the 14th external sleeve, the forces acting on the 1st internal sleeve, the input torque and the output torque) are presented in Figs. 3–7.

An increase in the number of consecutive defects leads to an increase in the force peaks during the analysis. The surface of the analysed external sleeve turns in contact with the surface of the defect, whose curvature radius is infinite. There is a rise of the contact force between the surface of the external sleeve and the surface of the cycloidal wheel, which can lead to a deepening of the wear. For the single wear defect, there is a single contact force peak of 600 N and another above 400 N, while in the cycloidal gearbox without defects, the contact force is lower than 200 N. For two consecutive defects, there are similar two peaks. For three, the number of force peaks increases to three (one peak with 600 N and two above 400 N). For 4 defects, there are two peaks above 700 N, three peaks of 600 N and two of 400 N. Increasing the number of defects to 5–7 lobes lead to 5–6 force peaks of 400–600 N. In the analysis with the artificial wear defect introduced in the 8 consecutive lobes, high amplitude oscillations of the dynamical entities appear in the first 0.12 s of analysis. These oscillations emerge after the locking of the cycloidal gearbox and originate in the contact modelling subroutines. After 0.13 s, the oscillations stabilize and the analysis is convergent.

There is little influence of the defects on the forces acting on the internal sleeves. For up to three consecutive defects of the lobes, there are little to no differences relative to the cycloidal gearbox without defects. For 5 and more defects, oscillations with amplitude up to 50 N appear when the contact forces reach their maximum values. For the 8 defects of the consecutive lobes, high oscillations at the beginning stage of analysis appear as it was mentioned earlier. During the start of the gearbox,
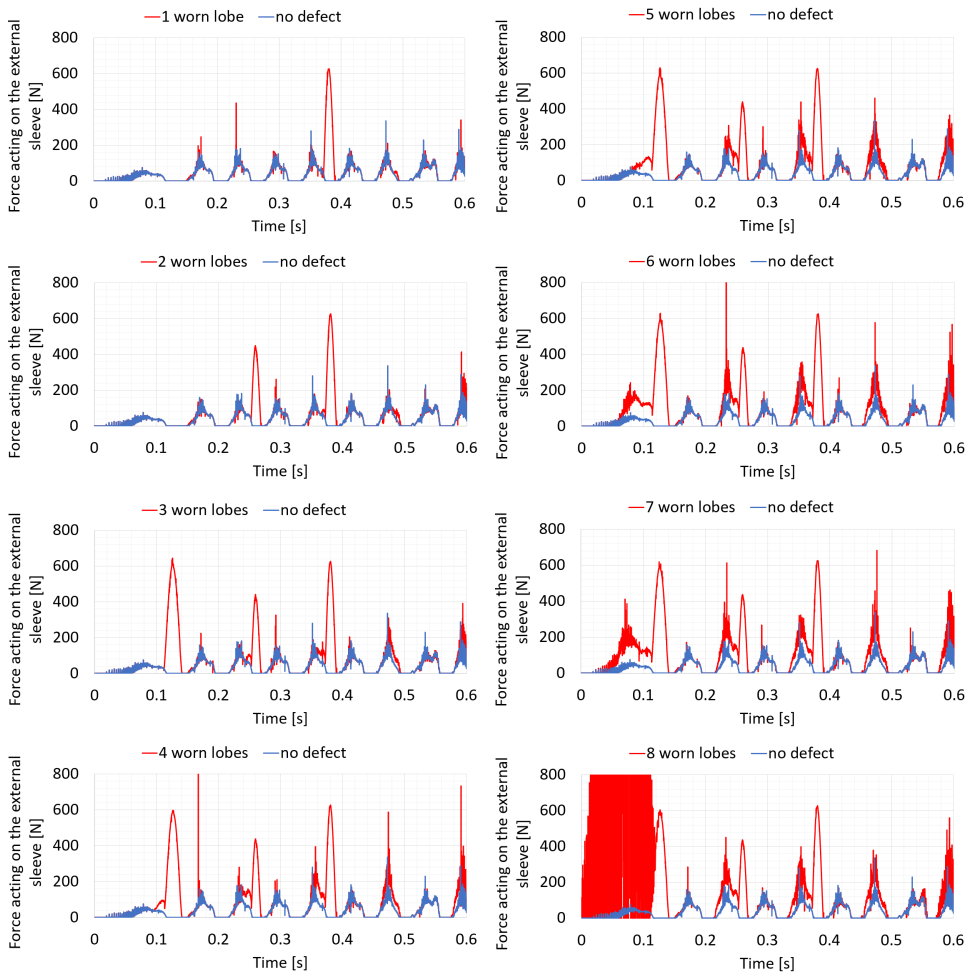
Fig. 3. Forces acting on the 14th external sleeve for the artificial wear defect introduced in the 1–8 consecutive lobes

the values of the forces acting on the internal sleeves in the model with defects are smaller than in the cycloidal gearbox without defects. The near-maximum value oscillations appear during work with stabilized angular velocity. The smaller value of the force acting at the 1st internal sleeve is related to the cycloidal wheel static force equilibrium equation (17).

$$\sum F_{in} + \sum F_{ex} + R = 0, \tag{17}$$

where: $\sum F_{in}$ – the sum of forces acting at the internal sleeves, $\sum F_{ex}$ – the sum of forces acting on the external sleeves, R – the reaction force at the cams of the input shaft, where cycloidal wheels are mounted.

The output shaft after the start of the cycloidal gearbox ($t > 0.2$ s) is loaded by the constant torque (10). The output loading torque imposes the reaction forces in the cams of the input shaft, on which cycloidal wheels are mounted. The force equilibrium (17) for the cycloidal wheel assumes that the reaction force R has an average value. Based on the R reaction force, torque at the input shaft (Fig. 5) was calculated. If we assume constant R, then the increase in the sum of forces acting on the external sleeves (Fig. 3) leads to a decrease in the forces acting on the internal sleeves (Fig. 4).
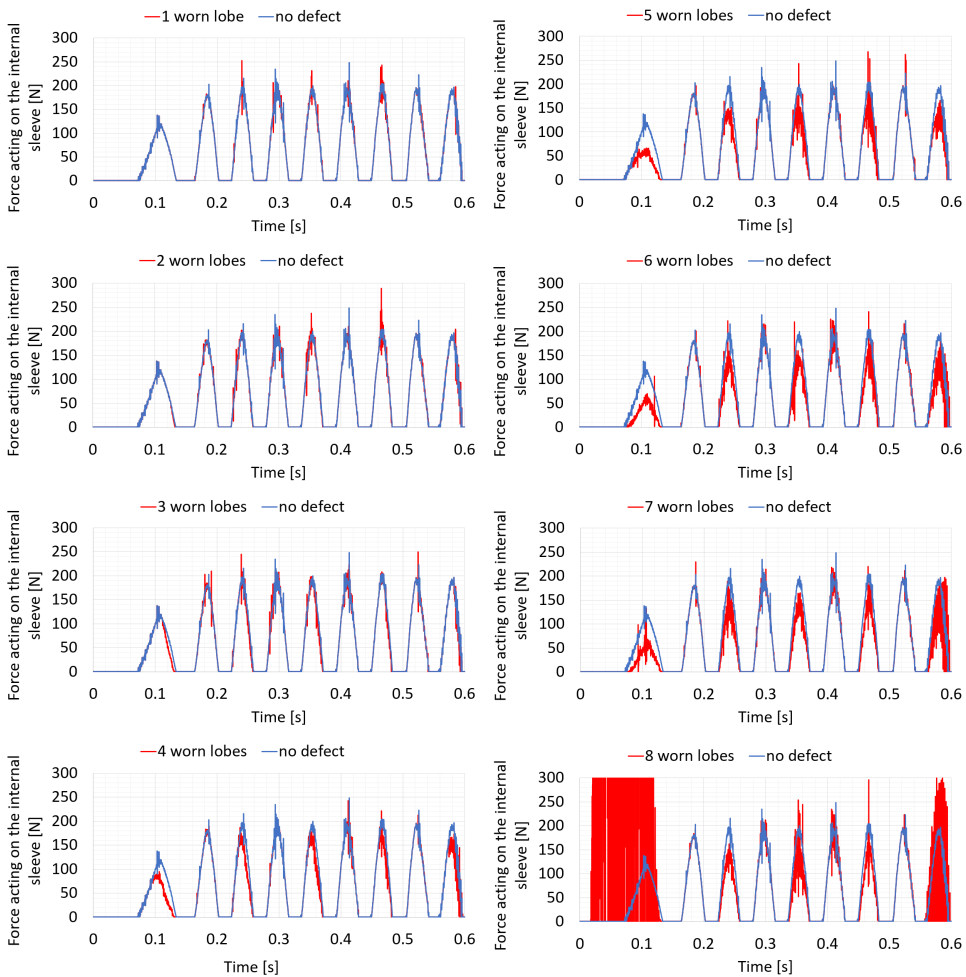
Fig. 4. Forces acting on the 1st internal sleeve for the artificial wear defect introduced in the 1–8 consecutive lobes

Torque at the input shaft has been calculated based on reaction forces in the centre points of two cams, on which cycloidal wheel bearings are mounted. The force pair is parallel and displaced by two eccentricities. The torque at the
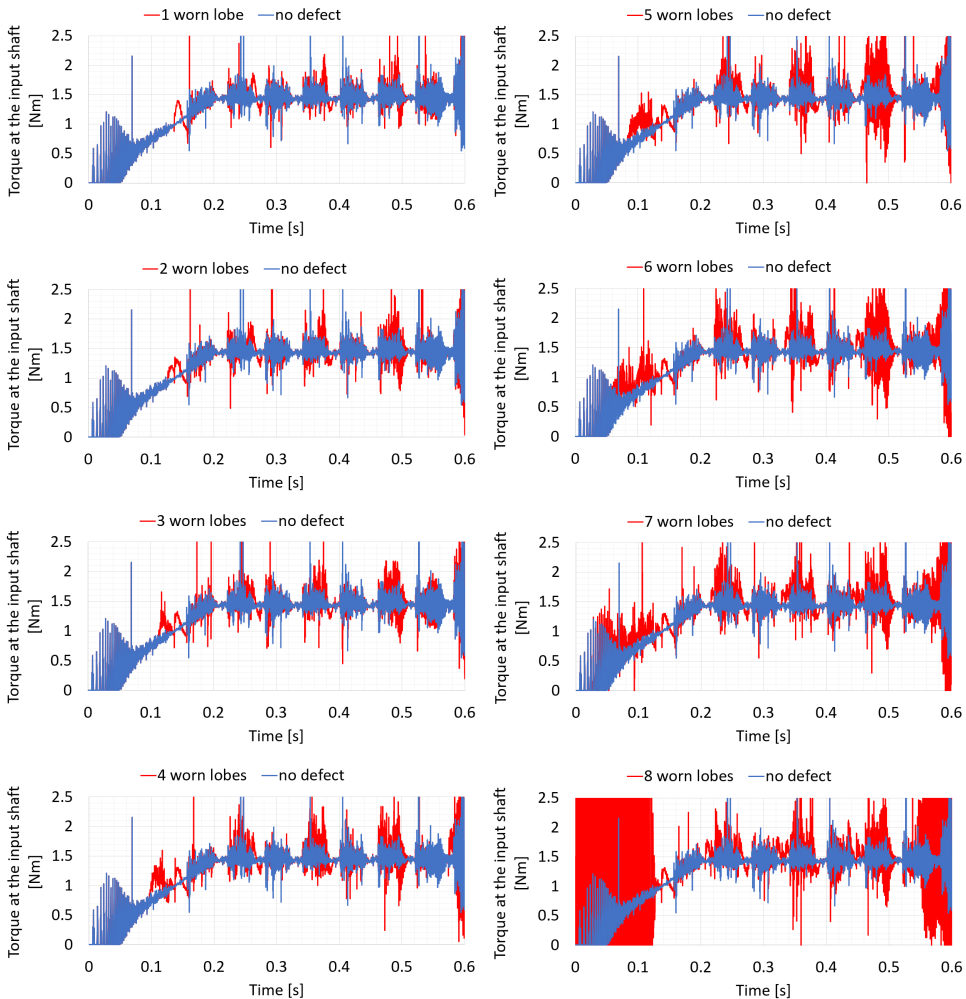
Fig. 5. Torque at the input shaft for the artificial wear defect introduced in the 1–8 consecutive lobes

input shaft increases the amplitude of vibration with the increase in the number of artificial wear defects of the consecutive lobes. However, it is difficult to distinguish between the intensity of vibrations for the 5 or more defects. The calculated torque is a random signal, which rises and falls in amplitude in unpredictable periods. This property of the cycloidal gearbox leads to difficulties in the formulation of the fault diagnosis methods. It is possible to find force peaks specific for the given defect in the time course of the contact forces, but it is difficult to extract features, which contain information about defects, from the input torque time course.

It was mentioned in the description of the contact forces that high amplitude oscillations appear in the beginning stage of the analysis, in the time course of the input torque.
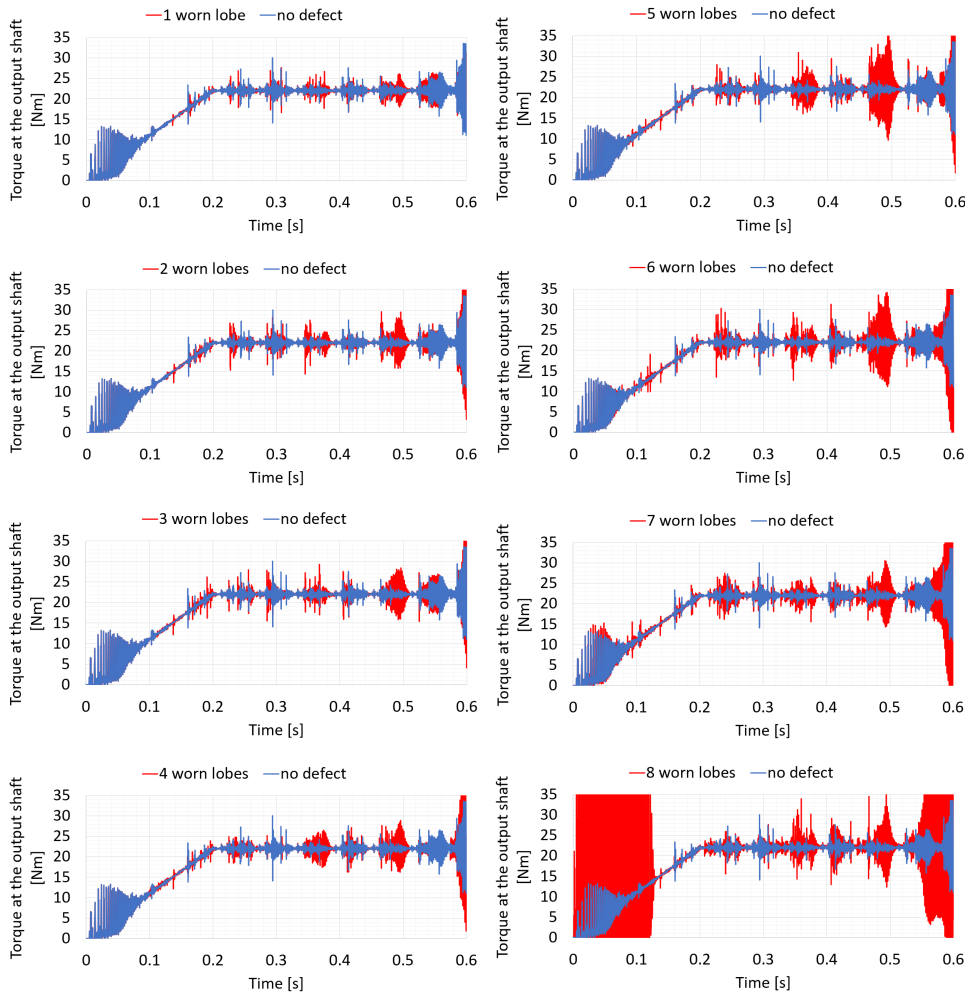
Fig. 6. Torque at the output shaft for the artificial wear defect introduced in the 1–8 consecutive lobes

In the time course of the torque at the output shaft (Fig. 6), the highest amplitude of vibrations arises in the models with artificial wear defects of the 5, 6 and 8 consecutive lobes. The amount of fluctuations rises for the models with defects of 1, 2, 3 and 4 consecutive lobes. However, it is difficult to find strict rules, which allow us to extract features which concern defects from the time course of the output torque and use them in the automatic fault diagnosis algorithm.

The enlarged period of the torque at the output shaft shown in Fig. 7 presents the random distribution of the increased amplitude periods. The amplitude of the output torque is higher for the greater number of defects in general, but it is still difficult to reveal how the output torque time course is exactly affected by the defect in the given lobe.
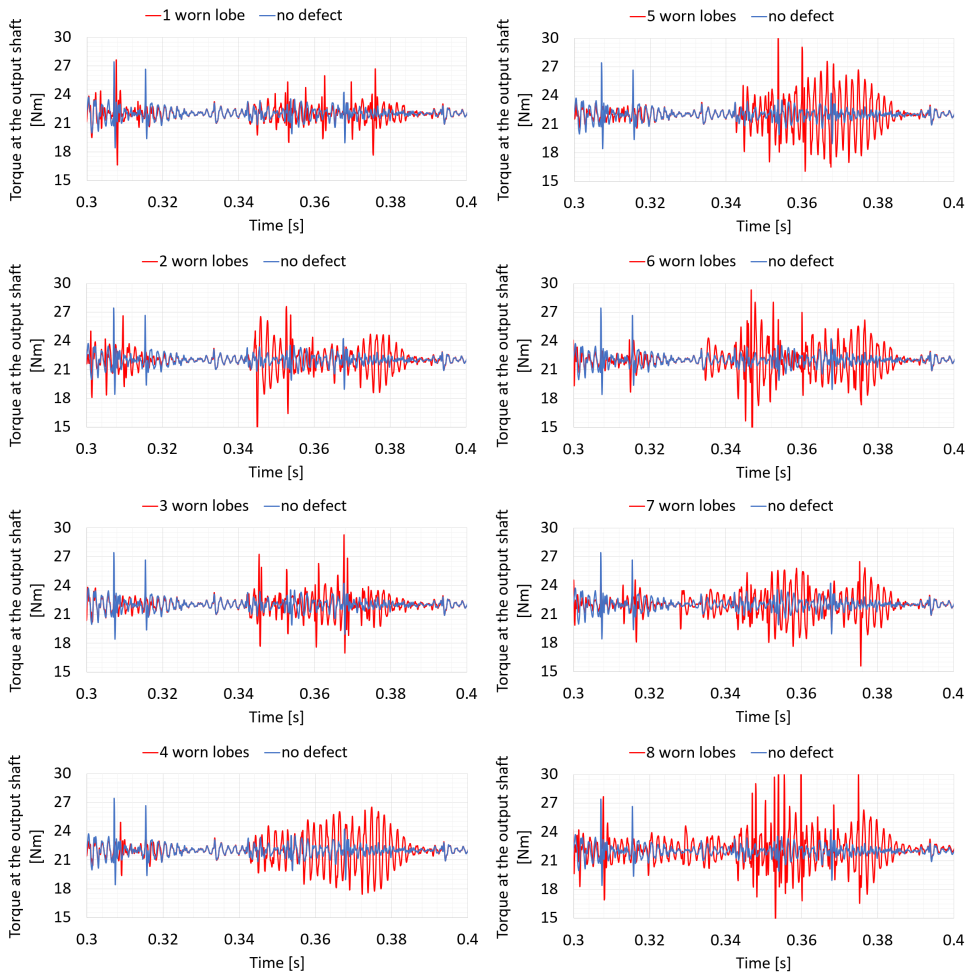
Fig. 7. Torque at the output shaft for the artificial wear defect introduced in the 1–8 consecutive lobes (enlarged time scope 0.3–0.4 s)

Time courses of the input and output torques can be studied using the coherence function, which will show how these entities could be affected by the defects of the lobes. The discrete wavelet transform can be also investigated to show the changes in the frequency components over the analysis time.

5. Spectral analysis of the torque at the output shaft for the cycloidal gearbox with artificial wear defects

The coherence function is defined in (18). If the frequency components of the torque from the healthy gearbox and from the gearbox with defects are equal, the coherence function value is 1.0. Differences in the spectral components of the

signals lead to the smaller than 1.0 value of the coherence function.

$$C_{xy}(f) = \frac{\left|S_{xy}(f)\right|^2}{S_{xx}(f)S_{yy}(f)}\,,\tag{18}$$

where: C_{xy} – magnitude-square coherence of the signals $x(t)$ and $y(t)$, S_{xy} – cross-spectral density of the signals $x(t)$ and $y(t)$, S_{xx}, S_{yy} – spectral density of the signals $x(t)$ and $y(t)$ respectively.

The time courses of the input torque and the output torque have been calculated in the analysis with the time 0.6 s and time step $\Delta t = 10^{-5}$ s. The coherence function has been calculated using the default MATLAB library of functions [26]. Figs. 8 and 9 show values of the coherence functions for the input and the output torques respectively, for the frequency range 0–1500 Hz.
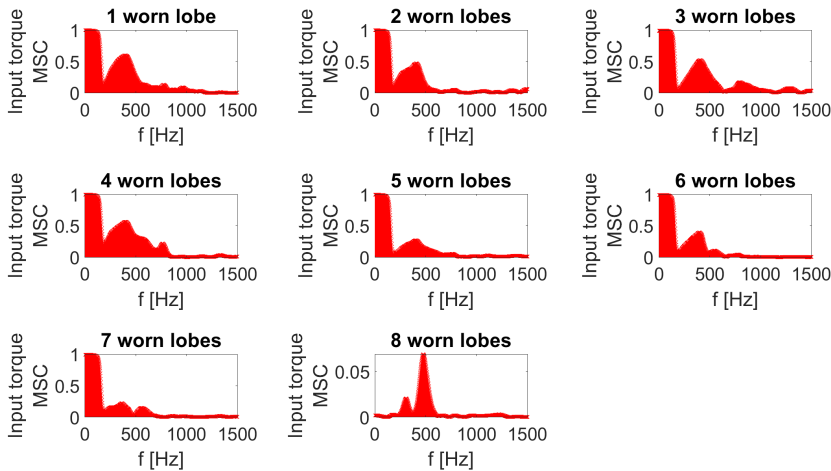
Fig. 8. Magnitude-squared coherence (MSC) of the input torque in the healthy cycloidal gearbox and in the cycloidal gearbox with the artificial wear defect in the 1–8 consecutive lobes

Calculation of the magnitude-square coherence for the two torques does not show dependence between the number of defects and affected frequency beans. For the input torque (Fig. 8), the coherence diagram for the defect in 4 consecutive lobes is more coherent with the input torque in the healthy gearbox than the diagram for defects of 2 or 3 consecutive lobes. For the output torque (Fig. 9) the diagrams for the 2, 5 and 6 worn lobes show small values of coherence in the range of 500-600 Hz, which is absent in the diagrams for the 3 and 4 worn lobes.

The DFT (Discrete Fourier Transform) do not show changes in the spectral components over time. The solution of the wavelet scalograms can improve the investigation of the torque features affected by the artificial wear defects. The author used 130 kinds of wavelets from the MATLAB default library [27]. Scalograms of these wavelets showed various time-frequency characteristics. The most interesting

www.czasopisma.pan.pl   PAN   www.journals.pan.pl
POLSKA AKADEMIA NAUK

Analysis of the single stage cycloidal gearbox with lobe defects. Fault diagnosis. . .   423
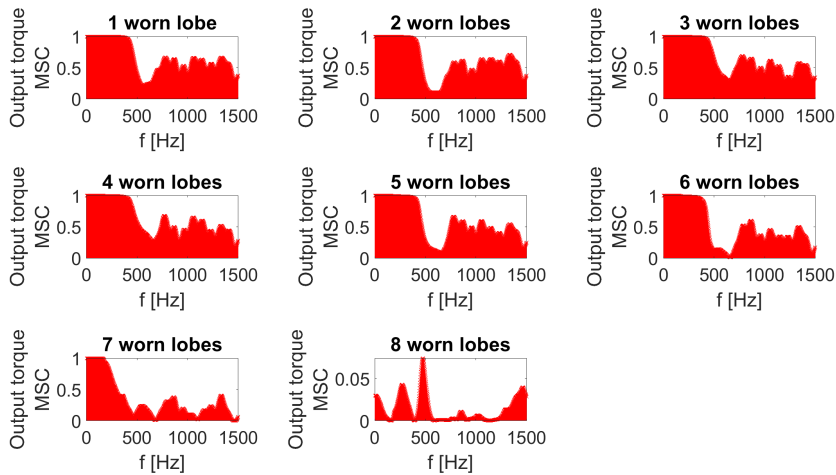
Fig. 9. Magnitude-squared coherence (MSC) of the output torque in the healthy cycloidal gearbox and the cycloidal gearbox with the artificial wear defect in the 1–8 consecutive lobes

results have been obtained for the *mb32.3* group of wavelets. The Discrete Wavelet Transform has been solved and Discrete Transform Absolute Coefficients have been shown for the output torque in the models with 1–8 consecutive worn lobes (Figs. 10 and 11). To analyse the influence of artificial wear defects, the variants of the models with random order of defects have been studied (Fig. 12). The Discrete Transform Absolute Coefficients have been shown for 12 levels, where the 1st level
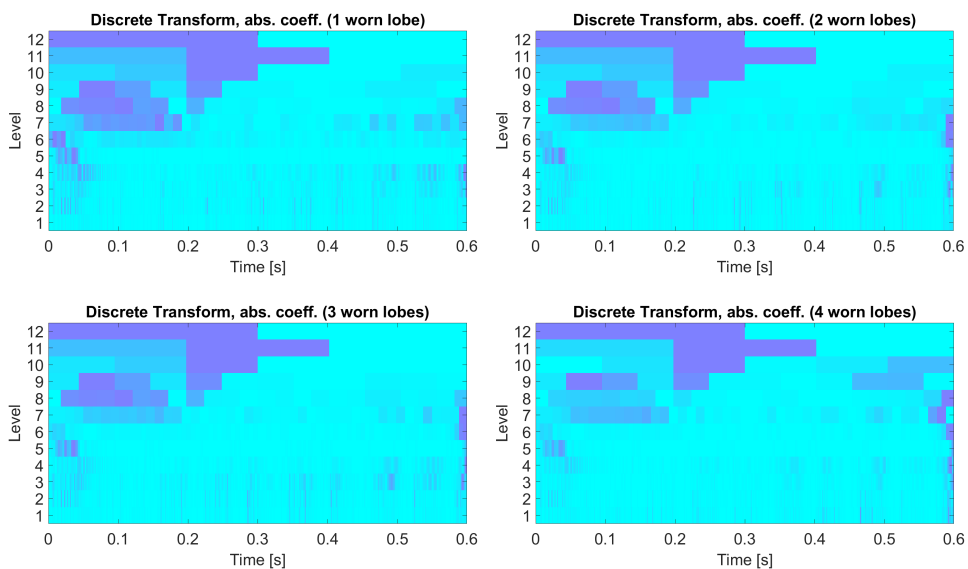
Fig. 10. Wavelet group mb32.3 scalograms of the output torque for the artificial wear defects of 1–4 consecutive lobes

corresponds to the highest frequencies and the 12th level corresponds to the lowest frequencies.
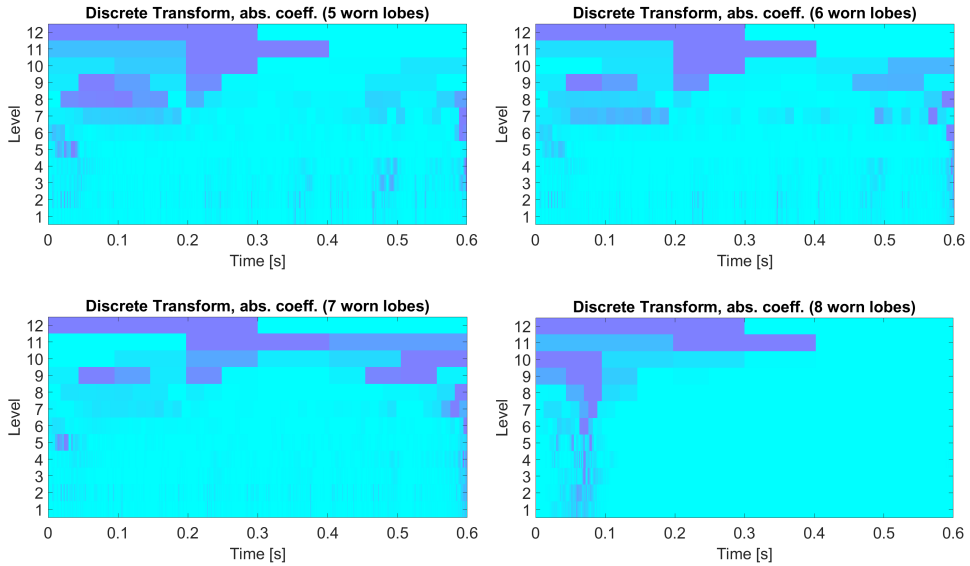
Fig. 11. Wavelet group mb32.3 scalograms of the output torque for the artificial wear defects of 5–8 consecutive lobes
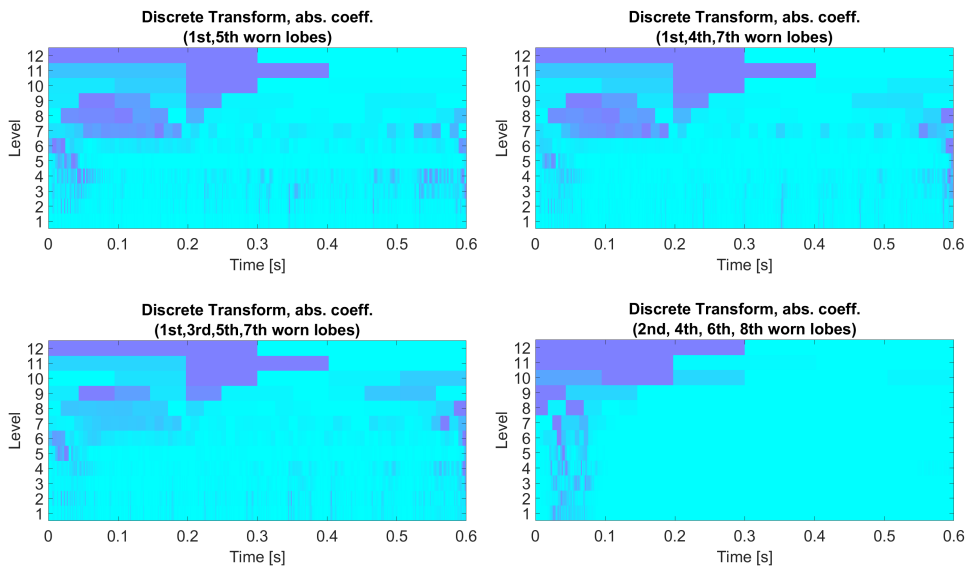
Fig. 12. Wavelet group mb32.3 scalograms of the output torque for the artificial wear defects of the random order of lobes

The highest value of the discrete transform absolute coefficient is designated by the darkest colour, while the smallest value is by the brightest. The colour scale has been set to 64 colour levels from the brightest: 1, to the darkest: 64.

6. New designs of the cycloidal gearbox based on the spectral analysis results

The scalogram for the 7 consecutive worn lobes shows a reduction in high frequencies for levels 1–4 (Fig. 11). Therefore, two new designs of the cycloidal gearbox have been tested. The first design is the design with 7 consecutive lobes completely removed from both cycloidal wheels (Fig. 13). The second design is with 7 consecutive lobes removed in the single cycloidal wheel (Fig. 14).
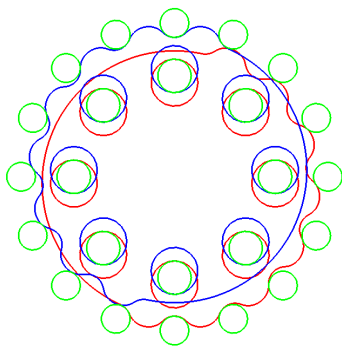
Fig. 13. New design of the cycloidal gearbox with 7 consecutive lobes removed in both cycloidal wheels
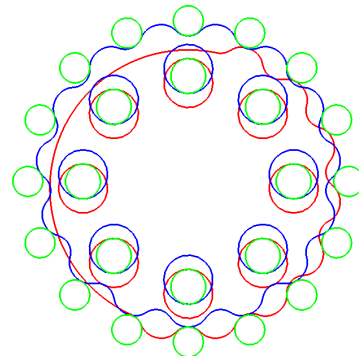
Fig. 14. New design of the cycloidal gearbox with 7 consecutive lobes removed in the single cycloidal wheel

Performed analyses showed that the mechanism of the cycloidal gearbox with 7 consecutive lobes removed in both wheels has been locked. Successful analysis has been performed for the model with 7 consecutive lobes removed in the single wheel (Fig. 14). The results of the analysis are very promising (Fig. 15). The model with the lobes removed in the single wheel has lower vibrations during the start in the input and output torques in the time range of 0–0.1 s. The cost of this design is increased forces acting on the internal sleeves every 2nd rotation of the input shaft. The values of these forces are 30% higher. When in one of the cycloidal wheels only a single lobe exerts force on the external sleeve, the output loading torque (10) acts on only half of the internal sleeves number, which imposes greater forces on these sleeves. However, the main advantage is that in the model with a complete set of lobes, the loading of the internal sleeves occurs twice as often as in the gearbox with the number of teeth reduced in the single cycloidal wheel.

The 8192-point DFT (Discrete Fourier Transform) with Hamming window has been computed for the output torque in the cycloidal gearbox with complete set
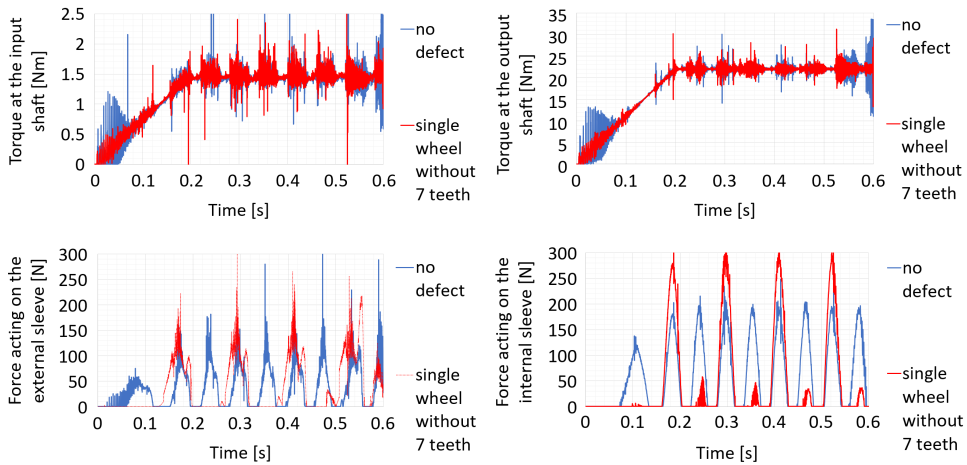
Fig. 15. Dynamical parameters of the cycloidal gearbox in the model with 7 consecutive lobes removed in the single cycloidal wheel

of the lobes and in the cycloidal gearbox with 7 consecutive lobes removed in the single wheel (Figs. 16 and 17).
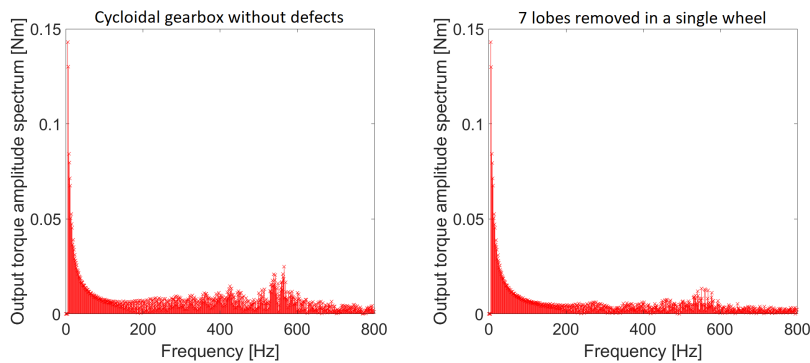
Fig. 16. DFT of the output torque in the gearbox with a complete set of the lobes (left) and in the gearbox with the 7 consecutive lobes removed in the single wheel (right)

It can be seen in Figs. 16 and 17 that in the new design of the cycloidal gearbox with 7 consecutive lobes removed in the single wheel, the amplitudes of the spectral components in the range of 200–800 Hz are twice as lower as in the cycloidal gearbox with a complete set of lobes, which proves that using of the Morris minimum-bandwidth wavelets could reveal important spectral properties of the cycloidal gearbox.
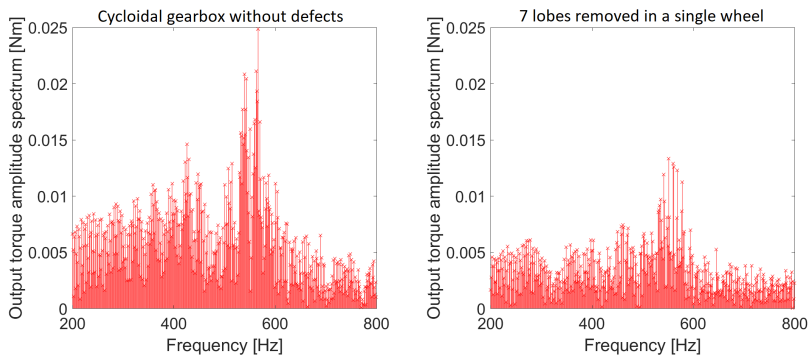
Fig. 17. Enlarged DFT diagram for the gearbox with a complete set of the lobes (left) and
for the gearbox with 7 consecutive lobes removed in the single cycloidal wheel

7. Application of the Morris minimum-bandwidth wavelets in the fault diagnosis

The scalograms in Figs. 10–12 could be used in the development of the new designs of the cycloidal gearboxes, where it is possible to eliminate vibrations with increased amplitude in the chosen periods. The main aim of the research presented in the current article is development of the fault diagnosis methods. Various scalograms for the wide group of wavelets were studied. It was found that for the Morris 'mb32.3' wavelets there is a gradual rise in the range of the eliminated frequencies for the successive rise in the artificial wear defects of the lobes. Levels 3 and 4 of the discrete wavelet transform absolute coefficients show this dependence, while for the other levels, the dependence does not appear. The scalogram shown in Fig. 18 has been prepared using a different method than those used in Figs. 10–12. The analysis for the artificial wear defects of the 8 consecutive lobes showed a high rise in the vibration amplitude at the beginning of the output torque time course. When the number of defects of the lobes increases, the analyses for the defects of the 1–7 consecutive lobes did not contain excessive vibration amplitudes, therefore scalograms of the output torques for analyses with defects of the 1–6 consecutive lobes have been compared with the analysis for the defect in the 7 consecutive lobes. In Fig. 18, the dark colour appears in the scalogram, if the absolute coefficients of the discrete wavelet transform for the given level contain the lowest possible value (the frequency bean does not exist) both in the scalogram for the 7 consecutive lobes and for the scalogram with the compared configuration of defects. In general, there is an increase in the area of the fields containing dark colour with the increase of the number of defects, which can be used in fault diagnosis to predict the number of damaged lobes. Unfortunately, the dependence is not fully reliable, as diagrams for the defects of the 3 and 4 consecutive lobes contain more gaps in the dark colour fields.
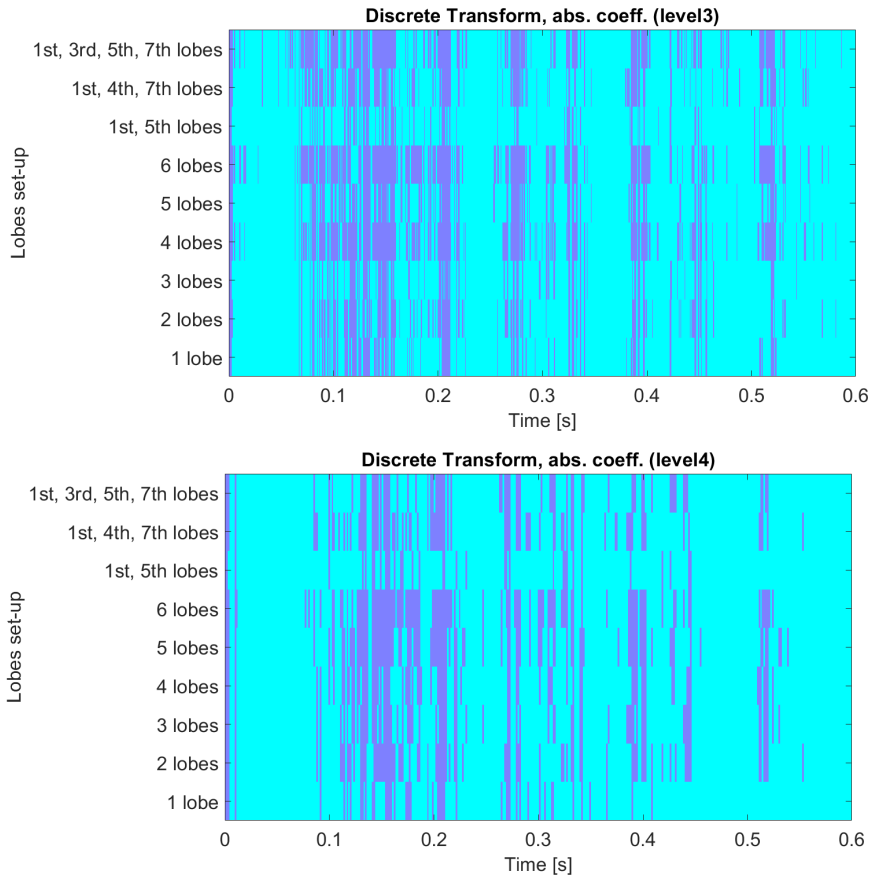
Fig. 18. Comparison scalograms of the discrete wavelet transform ('mb32.3') of the output torque
arising by the selection of lowest amplitude values (dark colour), which overlap with the low
amplitude values in the scalogram for the artificial lobe defects of the 7 consecutive lobes

8. Discussion of the results

The coherence function and Morris minimum-bandwidth wavelets can show differences in the torques from the healthy cycloidal gearbox and the cycloidal gearbox with defects. Unfortunately, it needs further research to reveal features of the calculated or measured signals in this kind of mechanism to accurately distinguish between the kind of defect or to show its exact localization.

The multibody dynamics model of the cycloidal gearbox [8] allows for the analysis of the various dynamic parameters including contact stiffness and contact damping. It can be used to investigate the influence of backlash or the most sophisticated kinds of defects of the cycloidal wheels, sleeves or shafts. It is also a reliable tool to investigate fault diagnosis methods giving the possibility to study the influence of the various imperfections on the spectral characteristics of the dynamic entities in the cycloidal gearbox.

The use of the correct contact modelling methods in the cycloidal gearbox needs further studies, which will eliminate excessive vibrations arising in the various ranges of time in the numerical analysis. Application of the Hunt and Crossley contact model with the improvements coming from the use of the Heaviside function guarantees the elimination of the sudden changes in the values of the contact stiffness and contact damping. To perform accurate studies of the dynamical phenomenon in the cycloidal gearbox, more precise contact modelling methods are needed. Random characteristic of the output and input torques is significantly affected by the energy dissipation in the contact model, which energy is difficult to measure in the cycloidal gearbox [28].

Defects of the cycloidal gearbox lobes lead to the emergence of disturbances in the form of peaks in the time courses of the forces and torques in the studied model. In general, the greater the number of defects, the more peaks appear during the work of the gearbox. Unfortunately, it is difficult to find any linear or accurate qualitative dependencies between the number of defects and the time courses or spectrums of forces acting on the sleeves or the torques at shafts.

The coherence functions are unique for each number of defects (Figs. 8 and 9). However, the shape of the frequency beans does not show any gradual dependence, which would allow us to find the features identifying defects of the calculated dynamic entities.

A discrete wavelet transform is a successful tool in finding features of the torques, which identify the specified defects. It shows frequency component changes in time. Using Morris minimum-bandwidth wavelets with image processing can lead to invention of the successful fault diagnosis methods in the cycloidal gearboxes. High amplitude oscillations in the output torque in the time range of 0–0.1 s are present in the scalograms (Figs. 10–12). It can be found as a circular shape in the time range 0–0.2 s at levels 7–9. It should be noted that among a tested group of wavelets, only the *mb32.3* group shows these features. Further research is needed to modify existing or find suitable wavelet transform to show disturbances of the output torque, which identify artificial lobe defects.

Fig. 11 shows a lack of vibrations at levels 3 and 4 for the artificial wear defects of the 7 consecutive lobes. The attempts to remove 7 lobes in a single cycloidal wheel allowed for the invention of the new design, which is characterized by the reduction of vibrations. The dynamical entities' characteristics confirmed (Figs. 15–17), that the use of Morris minimum-bandwidth wavelets successfully represents various features of the output torque, which can be exploited in the formulation of the fault diagnosis methods.

9. Conclusions

The multibody dynamics model of the cycloidal gearbox [8] allows for fast and versatile analysis. It is possible to study the influence of the various gearbox modifications on the dynamic parameters. Morris minimum-bandwidth wavelets

from the MATLAB library can be used in the development of fault diagnosis methods. Unfortunately, the dependence between the number of damaged lobes and reduced frequencies is not confirmed to be reliable. This method needs further investigation and proves that the use of wavelets is very promising in the fault diagnosis of the cycloidal gearboxes. Further research will be performed, which concerns the application of the Morris minimum-bandwidth wavelets in the devices measuring output torque in the cycloidal gearbox laboratory stand.

References

[1] Y. Fu, X. Chen, Y. Liu, C. Son, and Y. Yang. Gearbox fault diagnosis based on multi-sensor and multi-channel decision-level fusion based on SDP. *Applied Sciences*, 12(15):7535, 2022. doi: 10.3390/app12157535.

[2] F. Xie, H. Liu, J. Dong, G. Wang, L. Wang, and G. Li. Research on the gearbox fault diagnosis method based on multi-model feature fusion. *Machines*, 10(12):1186, 2022. doi: 10.3390/machines10121186.

[3] I. Komorska, K. Olejarczyk, A. Puchalski, M. Wikło, and Z. Wołczyński. Fault diagnosing of cycloidal gear reducer using statistical features of vibration signal and multifractal spectra. *Sensors*, 23(3):1645, 2023. doi: 10.3390/s23031645.

[4] R. Król. Analysis of the backlash in the single stage cycloidal gearbox. *Archive of Mechanical Engineering*, 69(4):693–711, 2022. doi: 10.24425/ame.2022.141521.

[5] R. Król. Resonance phenomenon in the single stage cycloidal gearbox. Analysis of vibrations at the output shaft as a function of the external sleeves stiffness. *Archive of Mechanical Engineering*, 68(3):303–320, 2021. doi: 10.24425/ame.2021.137050.

[6] R. Król and K. Król. Multibody dynamics model of the cycloidal gearbox, implemented in Fortran for analysis of dynamic parameters influenced by the backlash as a design tolerance. *Acta Mechanica et Automatica*, 17(2):272–280, 2023. doi: 10.2478/ama-2023-0031.

[7] R. Król. Cycloidal gearbox model for transient analysis implemented in Fortran with constant time step 2nd order integrator. In: A. Puchalski, B.E. Łazarz, F. Chaari, I. Komorska, Z. Zimroz (eds) *Advances in Technical Diagnostics II. ICTD 2022. Applied Condition Monitoring*, pp. 63–74, vol. 21. Springer, Cham 2023. doi: 10.1007/978-3-031-31719-4_7.

[8] R. Król. Software for the cycloidal gearbox multibody dynamics analysis, implemented in Fortran. (Purpose: presentation of the results in the scientific article), 2023. doi: 10.5281/ZENODO.7729842.

[9] R. Król. Kinematics and dynamics of the two stage cycloidal gearbox. *AUTOBUSY – Technika, Eksploatacja, Systemy Transportowe*, . 19(6):523–527, 2018. doi: 10.24136/atest.2018.125.

[10] K.S. Lin, K.Y. Chan, and J.J. Lee. Kinematic error analysis and tolerance allocation of cycloidal gear reducers. *Mechanism and Machine Theory*, 124:73–91, 2018. doi: 10.1016/ j.mech mach theory.2017.12.028.

[11] L.X. Xu, B.K. Chen, and C.Y. Li. Dynamic modelling and contact analysis of bearing-cycloid-pinwheel transmission mechanisms used in joint rotate vector reducers. *Mechanism and Machine Theory*, 137:432–458, 2019. doi: 10.1016/j.mechmachtheory.2019.03.035.

[12] Y. Li, K. Feng, X. Liang, and M.J. Zuo. A fault diagnosis method for planetary gearboxes under non-stationary working conditions using improved Vold-Kalman filter and multi-scale sample entropy. *Journal of Sound and Vibration*, 439:271–286, 2019. doi: 10.1016/j.jsv.2018.09.054.

[13] S. Schmidt, P.S. Heyns, and J.P. de Villiers. A novelty detection diagnostic methodology for gearboxes operating under fluctuating operating conditions using probabilistic techniques. *Mechanical Systems and Signal Processing*, 100:152–166, 2018. doi: 10.1016/j.ymssp.2017.07.032.

[14] Y. Lei, D. Han, J. Lin, and Z. He. Planetary gearbox fault diagnosis using an adaptive stochastic resonance method. *Mechanical Systems and Signal Processing*, 38(1):113–124, 2013. doi: 10.1016/j.ymssp.2012.06.021.

[15] Y. Chen, X. Liang, and M.J. Zuo. Sparse time series modeling of the baseline vibration from a gearbox under time-varying speed condition. *Mechanical Systems and Signal Processing*, 134:106342, 2019. doi: 10.1016/j.ymssp.2019.106342.

[16] G. D'Elia, E. Mucchi, and M. Cocconcelli. On the identification of the angular position of gears for the diagnostics of planetary gearboxes. *Mechanical Systems and Signal Processing*, 83:305–320, 2017. doi: 10.1016/j.ymssp.2016.06.016.

[17] X. Chen and Z. Feng. Time-frequency space vector modulus analysis of motor current for planetary gearbox fault diagnosis under variable speed conditions. *Mechanical Systems and Signal Processing*, 121:636–654, 2019. doi: 10.1016/j.ymssp.2018.11.049.

[18] S. Schmidt, P.S. Heyns, and K.C. Gryllias. A methodology using the spectral coherence and healthy historical data to perform gearbox fault diagnosis under varying operating conditions. *Applied Acoustics*, 158:107038, 2020. doi: 10.1016/j.apacoust.2019.107038.

[19] D. Zhang and D. Yu. Multi-fault diagnosis of gearbox based on resonance-based signal sparse decomposition and comb filter. *Measurement*, 103:361–369, 2017. doi: 10.1016/j.measurement.2017.03.006.

[20] C. Wang, H. Li, J. Ou, R. Hu, S. Hu, and A. Liu. Identification of planetary gearbox weak compound fault based on parallel dual-parameter optimized resonance sparse decomposition and improved MOMEDA. *Measurement*, 165:108079, 2020. doi: 10.1016/j.measurement.2020.108079.

[21] W. Teng, X. Ding, H. Cheng, C. Han, Y. Liu, and H. Mu. Compound faults diagnosis and analysis for a wind turbine gearbox via a novel vibration model and empirical wavelet transform. *Renewable Energy*, 136:393–402, 2019. doi: 10.1016/j.renene.2018.12.094.

[22] D. Abboud, S. Baudin, J. Antoni, D. Rémond, M. Eltabach, and O. Sauvage. The spectral analysis of cyclo-non-stationary signals. *Mechanical Systems and Signal Processing*, 75:280–300, 2016. doi: 10.1016/j.ymssp.2015.09.034.

[23] J.M. Morris and R. Peravali. Minimum-bandwidth discrete-time wavelets, Signal Processing, vol. 76, no. 2, pp. 181–193, 1999. doi: 10.1016/S0165-1684(99)00007-9.

[24] R. Król. Software for the cycloidal gearbox multibody dynamics analysis, implemented in Fortran. (Purpose: presentation of the results in the scientific article), 2022. doi: 10.5281/ZENODO.7221146.

[25] P. Flores and H.M. Lankarani. *Contact Force Models for Multibody Dynamics*, vol. 226, Springer, 2016. doi: 10.1007/978-3-319-30897-5.

[26] MATLAB documentation, https://www.mathworks.com/help/signal/ref/mscohere.html.

[27] MATLAB documentation, https://www.mathworks.com/help/wavelet/ug/wavelet-families-additional-discussion.html.

[28] X. Shi and A.A. Polycarpou. Measurement and modeling of normal contact stiffness and contact damping at the meso scale. *Journal of Vibration and Acoustics*, 127(1):52–60, 2005. doi: 10.1115/1.1857920.